

Reconfigurable optical add-drop multiplexers for hybrid mode-/wavelength-division-multiplexing systems

Xiaolin Yi,^a Weike Zhao,^a Chenlei Li,^a Long Zhang,^a Yuluan Xiang,^a Chaoyue Liu,^a Yaocheng Shi,^{a,b} Liu Liu,^{a,b} and Daoxin Dai^{a,b,c,*}

^aZhejiang University, College of Optical Science and Engineering, Center for Optical and Electromagnetic Research,

International Research Center for Advanced Photonics, State Key Laboratory for Modern Optical Instrumentation, Hangzhou, China

^bZhejiang University, Ningbo Research Institute, Ningbo, China

^cZhejiang University, Jiaying Research Institute, Intelligent Optics and Photonics Research Center, Jiaying Key Laboratory of Photonic Sensing and Intelligent Imaging, Jiaying, China

Abstract. Dealing with the increase in data workloads and network complexity requires efficient selective manipulation of any channels in hybrid mode-/wavelength-division multiplexing (MDM/WDM) systems. A reconfigurable optical add-drop multiplexer (ROADM) using special modal field redistribution is proposed and demonstrated to enable the selective access of any mode-/wavelength-channels. With the assistance of the subwavelength grating structures, the launched modes are redistributed to be the supermodes localized at different regions of the multimode bus waveguide. Microring resonators are placed at the corresponding side of the bus waveguide to have specific evanescent coupling of the redistributed supermodes, so that any mode-/wavelength-channel can be added/dropped by thermally tuning the resonant wavelength. As an example, a ROADM for the case with three mode-channels is designed with low excess losses of <0.6, 0.7, and 1.3 dB as well as low cross talks of <−26.3, −28.5, and −39.3 dB for the TE₀, TE₁, and TE₂ modes, respectively, around the central wavelength of 1550 nm. The data transmission of 30 Gbps/channel is also demonstrated successfully. The present ROADM provides a promising route for data switching/routing in hybrid MDM/WDM systems.

Keywords: reconfigurability; hybrid multiplexing; subwavelength grating; silicon photonics.

Received Jul. 18, 2023; revised manuscript received Sep. 14, 2023; accepted for publication Oct. 8, 2023; published online Nov. 9, 2023.

© The Authors. Published by SPIE and CLP under a Creative Commons Attribution 4.0 International License. Distribution or reproduction of this work in whole or in part requires full attribution of the original publication, including its DOI.

[DOI: [10.1117/1.APN.2.6.066004](https://doi.org/10.1117/1.APN.2.6.066004)]

1 Introduction

Ever-growing data traffic has become a severe problem as cloud computing and artificial intelligence have developed in the past few decades, leading to an increasing demand for high-capacity transmissions.^{1,2} A key to solving this problem is exploiting optical interconnects to enhance the link capacity, which exhibit potential for high speed, broad bandwidth, and low power consumption.^{3–5} To realize high-capacity optical communications, multiplexing techniques have been widely investigated and utilized, including wavelength-

division multiplexing (WDM),^{6–8} polarization-division multiplexing (PDM),^{9–12} and mode-division multiplexing (MDM).^{13–15} Among them, the MDM technique has attracted substantial attention, as it leverages multiple orthogonal spatial modes as the carrier to transmit massive data in parallel within a single wavelength, which is promising to meet the rapidly increasing demand for high-capacity and low-cost optical interconnects.^{16,17}

With the development of the multiplexing technologies, multidimensional multiplexing systems have also gained popularity and hybrid MDM-WDM-PDM devices have been intensively investigated.^{18,19} For example, a WDM-compatible MDM system was carried out by employing single-mode microring resonators (MRRs) to couple different spatial modes into a

*Address all correspondence to Daoxin Dai, dxdai@zju.edu.cn

multimode waveguide.²⁰ Later, an on-chip MDM switch was proposed with full flexibility to enable networks with many nodes connected by high-bandwidth multimode links to dynamically allocate bandwidth, which is scalable with more mode-/wavelength-channels.²¹ A mode-selective modulation is realized by combining silicon MRRs and the mode multiplexer based on asymmetric directional couplers (ADCs), in which way the mode carriers in the multimode bus waveguide (MBW) can be selectively modulated.²² In recent years, reconfigurable optical add-drop multiplexers (ROADMs) have been widely proposed and demonstrated to enable any mode-/wavelength-channel to be switched and routed flexibly.^{23–25}

Despite the great efforts that have been made so far, the selective manipulation of individual optical carriers is still of particular interest because it aims to access a particular individual channel without introducing any undesired influences on other channels. In other words, any desired channels are able to be selectively added/dropped to/from the MBW. In 2021, an MDM switch was demonstrated so that any mode-/wavelength-channels can be directly accessed, but additional mode conversion devices were required to convert each mode into the highest-order mode supported by the MBW, which therefore increased the complexity.²⁶ In 2022, a three-mode (de)multiplexing device was demonstrated by introducing multimode MRRs, in which case the fundamental mode in the bus waveguide was evanescently coupled to the TE_1 mode in the Euler-based MRR.²⁷ Nevertheless, it suffered from excess loss (EL) and cross talk, hindering its practical applications. Recently, an MZI-based mode-sensitive phase shifter was proposed using subwavelength grating (SWG) structures to have varied temperature coefficients for different modes, which provided a new way for realizing the mode-selective phase manipulation with high extinction ratios.²⁸ So far, it still remains a challenge to selectively add/drop the target optical mode-channel individually without influencing the undesired channels flexibly.

In this paper, based on our previous work, we propose a ROADM for hybrid MDM/WDM systems by utilizing the

modal field redistribution to enable the efficient selective access of any mode-/wavelength-channels.²⁹ With the assistance of SWG structures to engineer the refractive index, the launched modes are redistributed to be the supermodes localized at different regions of the MBW. In this way, the evanescent coupling of the desired mode-channel can be enhanced, while the undesired mode coupling can be suppressed significantly. MRR-based wavelength-selective switches are placed at the side of the bus waveguide to have specific evanescent coupling for the corresponding redistributed supermodes. By tuning the resonant wavelength of the MRRs, any wavelength-channels can be switched flexibly and accessed selectively. With such devices, any target mode-/wavelength-channels can be easily added/dropped without affecting the other non-target channels. As an example, we design a ROADM with three mode-channels, which have low ELs of <0.6, 0.7, and 1.3 dB and low intermode cross talks of <−26.3, −28.5, and −39.3 dB around the resonant wavelength of ~1550 nm. For the fabricated device, the ELs for TE_0 , TE_1 , and TE_2 modes range from 0.6 to 2.7 dB over a broad wavelength range of 1530–1605 nm. The intermode cross talks are less than −23.9, −18.5, and −19.4 dB, respectively. Finally, the data transmission of 30 Gbps/channel is demonstrated successfully. The proposed ROADM is promising for data switching and routing in hybrid MDM/WDM systems in the future.

2 Principle and Design

Here, as proposed in our previous work, we propose a ROADM utilizing the scheme of redistributing the modal field in the MBW,²⁹ which enables the simultaneous manipulation of the evanescent coupling for all the mode-/wavelength-channels considered. In this case, we design a ROADM with three TE mode-channels as an example; the schematic configuration is shown in Fig. 1. The proposed ROADM consists of an SWG-structure-assisted MBW and three MRR-based wavelength-selective switches. As shown in Fig. 1, the SWG structure embedded in the MBW is used to engineer the equivalent refractive index

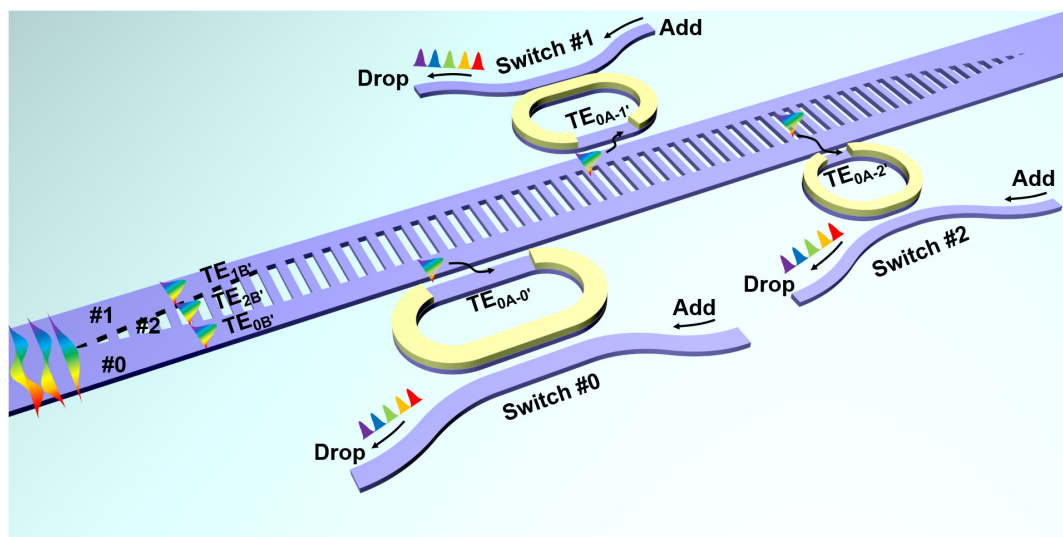


Fig. 1 3D illustration of the proposed ROADM utilizing the scheme of redistributing the modal fields. Here the launched TE_0 , TE_1 , and TE_2 modes are converted to the $TE_{0B'}$, $TE_{1B'}$, and $TE_{2B'}$ supermodes, whose modal fields are redistributed to be localized at regions #0, #1, and #2, respectively.

profile, so that the launched TE_0 , TE_1 , and TE_2 modes are converted to the $TE_{0B'}$, $TE_{1B'}$, and $TE_{2B'}$ supermodes whose modal fields are redistributed to be localized at regions #0, #1, and #2, respectively. Since these supermodes are orthogonal with different effective indices, they can be maintained across the SWG MBW without cross-coupling. Note that the supermodes are localized in the corresponding region with only one major peak. In this way, the coupling of the non-target mode-channels can be suppressed significantly, while that of the target mode can be enhanced. Particularly, an adiabatic SWG taper is introduced to realize efficient mode conversion from the uniform MBW to the coupling region with SWG structures. The MRR wavelength-selective switches #0, #1, and #2 are then placed at the corresponding side of the MBW to have efficient evanescent coupling for the target supermodes ($TE_{0B'}$, $TE_{1B'}$, and $TE_{2B'}$ modes), so that any mode-channels can be added/dropped selectively and flexibly. By tuning the resonant wavelengths of the MRRs, different wavelength-channels can be switched and accessed selectively. Here microheaters are introduced for thermally tuning the resonant wavelength of each MRR switch. For switches #0, #1, and #2, data carried by different wavelength-channels ($\lambda_1, \lambda_2, \dots, \lambda_N$) of three mode-channels in the MBW can be dropped selectively. Similarly, the local data carried by different wavelength-channels ($\lambda_1, \lambda_2, \dots, \lambda_N$) can also be added from the add port of the corresponding MRR switch to the target mode-channel in the MBW. With such a ROADM, one can selectively add/drop any mode-/wavelength-channels to/from the MBW by simply tuning the resonant wavelength of the MRR switch, which is promising to be further used for other applications in hybrid MDM/WDM systems. Notably, it is possible to be scaled for working with more mode-channels,

because higher-order modes have weaker mode confinement and thus are easier to be added/dropped when using optimally designed ADCs. In addition, it is also possible to develop ROADMs working with the mode-channels of dual polarizations (including both TE_i and TM_i modes) according to the operation mechanisms of the adiabatic SWG tapers and the MRRs.

Here the present ROADM is designed on the silicon-on-insulator (SOI) platform with a 220-nm-thick top silicon layer and a 2- μm -thick buried oxide layer. The operation wavelength is around 1550 nm, and the corresponding refractive index of silicon and silica are $n_{\text{Si}} = 3.476$ and $n_{\text{SiO}_2} = 1.444$, respectively. The key parameters of the MRR switch are shown in Fig. 2(a), where the Ti/W alloy heater is deposited on the silica upper cladding above the MRRs for tuning the resonant wavelength, as shown in Fig. 2(b).

The MBW width w_b is chosen as 1.5 μm to support the TE_0 , TE_1 , and TE_2 modes. The period and the duty cycle of the SWG structure are chosen as $\Lambda = 210$ nm and $f = 0.5$ according to the subwavelength-regime condition³⁰ and the requirement of the fabrication process. The end widths (w_0 , w_1 , and w_2) of regions #0, #1, and #2 are, respectively, chosen as (0.4, 0.3, and 0.8 μm), so that the redistributed supermodes are localized at the desired local regions of the MBW.²⁹ Figures 3(a)–3(c) show the simulated light propagation in the SWG mode evolution region and the redistributed modal fields of the $TE_{0B'}$, $TE_{1B'}$, and $TE_{2B'}$ supermodes, respectively. It can be seen clearly that these three supermodes are localized well at regions #0, #1, and #2 in the MBW as desired.

The coupling region of the MRR switches is designed carefully, so that different mode-/wavelength-channels can be selectively added/dropped. Figure 4(a) shows the calculated

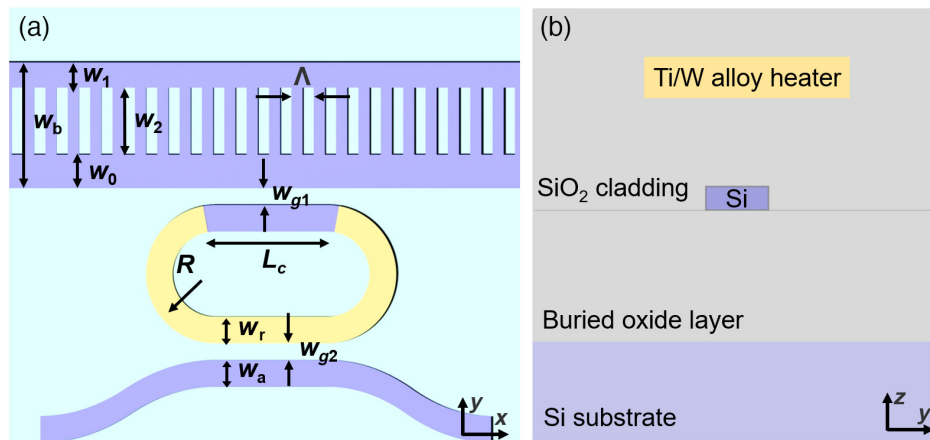


Fig. 2 Details of the MRR. (a) Coupling region of the thermally tunable MRR switch. (b) Cross section of the SOI photonic waveguide with a microheater on the top.

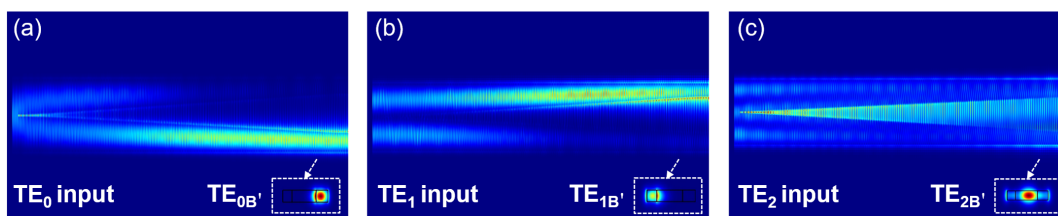


Fig. 3 Design of the SWG mode evolution region. Simulated light propagation in the SWG MBW and the redistributed modal fields of the (a) $TE_{0B'}$, (b) $TE_{1B'}$, and (c) $TE_{2B'}$ supermodes, respectively.

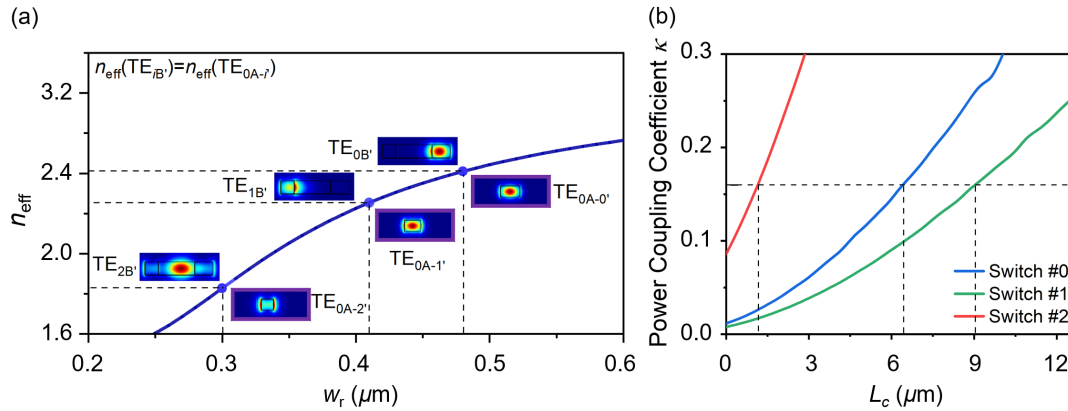


Fig. 4 Design of the microring waveguide. (a) Calculated effective indices of the supermodes and the fundamental modes of each MRR waveguide as w_r varies. (b) Calculated power coupling coefficient for three MRRs as the coupling length L_c varies. Here the coupling length is defined as $L_c = N\Lambda$, where N is the period number of the grating.

effective index of the modes as the width w_r of the microring waveguide varies. The width w_r and the access waveguide width w_a for switches #0, #1, and #2 are chosen as 476, 410, and 300 nm according to the phase-matching condition given as $n_{\text{eff}}(\text{TE}_{iB'}) = n_{\text{eff}}(\text{TE}_{0A-i'})$, respectively.²⁹ In particular, the racetrack MRRs are used for the flexible manipulation of the coupling ratios. The 3-dB bandwidth is chosen to be as large as 0.8 nm (100 GHz), so that data transmission of up to 100 Gbps/channel can potentially be achieved. Accordingly, the power coupling coefficient κ is optimally chosen as ~ 0.16 based on the transfer matrix method (TMM). Figure 4(b) shows the calculated power coupling coefficients κ for three MRRs as the coupling length L_c varies. The length of the coupling region is defined as $L_c = N\Lambda$, where N is the period number of the grating. Here the widths w_{g2} of the gaps between the access waveguide and the ring waveguide are, respectively, chosen as 0.20, 0.315, and 0.43 μm for the three channels, which are sufficiently large for fabrication ease. Correspondingly, the coupling lengths L_c are chosen as 6.30, 8.82, and 1.05 μm to achieve the optimal coupling ratio, respectively. Similarly, the widths w_{g1} of the gaps between the MBW and the microring waveguides are chosen as 0.195, 0.290, and 0.305 μm to realize the optimal coupling ratio.

The free spectral range (FSR) of the present MRR is given as

$$\text{FSR} = \frac{\lambda^2}{n_g(2\pi R + 2L_c)}, \quad (1)$$

where λ is the operating wavelength, n_g is the group index of the guided mode, and R is the bending radius of the resonator. The bending radius R should be chosen optimally to achieve low ELs and large FSRs. Notably, the bending radius for the MRR should be minimized to maximize the FSR so that more

wavelength-channels are available, while it is limited due to the bending loss. As a trade-off, the FSR is designed to be ~ 15.8 nm to cover four wavelength-channels with a channel spacing of 400 GHz ($\Delta\lambda = 3.2$ nm) by choosing the bending radius R of the three MRRs as 3.94, 3.21, and 5.62 μm , so that their central resonant wavelengths are aligned to 1550 nm. All the designed key parameters are summarized in Table 1.

A three-dimensional finite-difference time-domain (3D-FDTD) method is used to simulate the transmission and light propagation of the MRR switches. For switches #1 and #2 used for the TE_1 and TE_2 mode-channels, the MRRs are placed at the sides of regions #1 and #0, respectively, as shown in Fig. 1. Figures 5(a)–5(c) show the simulated light propagation for the designed switch # i ($i = 0, 1, \text{ and } 2$) (including the mode conversion region and the mode coupling region) at the resonant wavelength of 1550 nm when the TE_i ($i = 0, 1, \text{ and } 2$) mode is launched in the MBW, respectively. It is clear that the mode profile of the launched TE_i mode is redistributed and finally converted to supermodes $\text{TE}_{iB'}$ localized at region # i of the MBW ($i = 0, 1, \text{ and } 2$). The supermodes launched at the input end of the corresponding switch are selectively evanescently coupled to the corresponding MRR with different resonant wavelength-channels. It can be seen that the designed ROADM works well with all the desired mode-/wavelength-channels.

Figures 5(d)–5(f) show the calculated transmissions at the drop port of the whole ROADM structure for the TE_0 , TE_1 , and TE_2 mode-channels. It shows that the switch has a low EL of $< 0.6, 0.7, \text{ and } 1.3$ dB and low intermode cross talk of $< -26.3, -28.5, \text{ and } -39.3$ dB for the TE_0 , TE_1 , and TE_2 mode-channels, respectively, around the central resonant wavelength of 1550 nm. These mode-channels have ELs of $< 0.6, 0.8, \text{ and } 1.7$ dB and intermode cross talk of $< -24.7, -25.2, \text{ and } -31.3$ dB in the wavelength range of 1500–1590 nm, respectively. Notably, the FSRs of these MRRs are as large as

Table 1 Structure parameters.

Channel	R (μm)	w_r (nm)	w_a (nm)	w_{g1} (nm)	w_{g2} (nm)	L_c (μm)
TE_0	3.94	476	476	195	200	6.30 ($N = 30$)
TE_1	3.21	410	410	290	315	8.82 ($N = 42$)
TE_2	5.62	300	300	305	430	1.05 ($N = 5$)

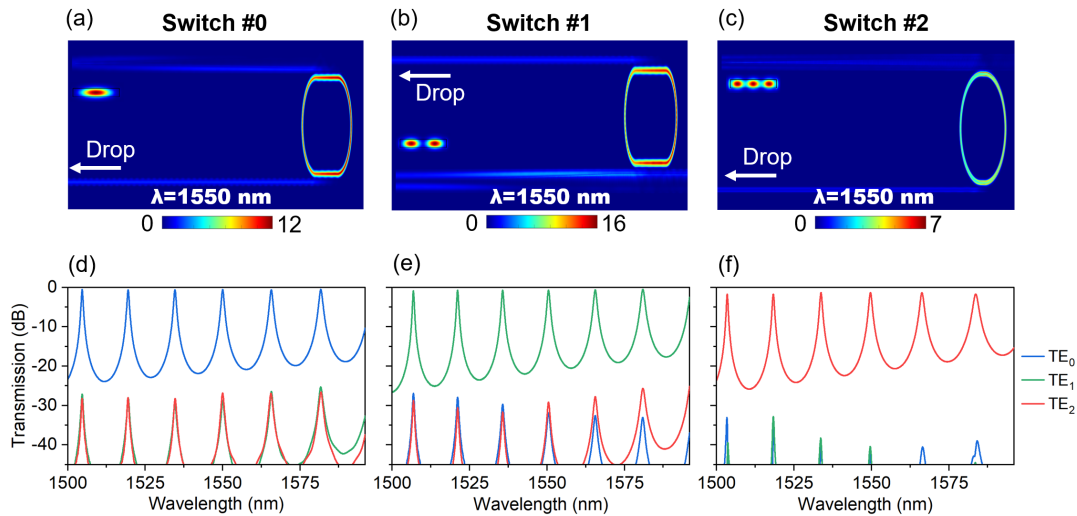


Fig. 5 Simulation results for the designed switches. Simulated light propagation for switch (a) #0, (b) #1, and (c) #2 at the resonant wavelength of 1550 nm when the TE_0 , TE_1 , and TE_2 modes are launched in the MBW, respectively. Here the mode conversion region and the mode coupling region are included. Calculated transmissions at the drop port of the whole ROADM structure for the (d) TE_0 , (e) TE_1 , and (f) TE_2 mode-channels.

15.72, 15.08, and 16.60 nm for switches #0, #1, and #2, respectively, which are slightly different from the designed values. The intermode cross talk can be further reduced by carefully optimizing the waveguide width and the gap width of the MRRs for maximizing the mode mismatch and lowering the evanescent coupling for those mode-channels that are not desired to be added/dropped.

The fabrication tolerance of the designed MRR switches is also analyzed by varying the core width w_r of the MRR waveguides, as shown in Figs. 6(a) and 6(b). Consider that the simulation for the whole ROADM structure is time-consuming when using the 3D-FDTD method, so the TMM method is chosen to be used here for the analysis. The simulation result indicates that there is no notable deterioration on either the EL or the intermode cross talk for these MRR switches. By utilizing the modal field redistribution method, the undesired mode coupling can be suppressed significantly and any target mode-/wavelength-channels can be selectively added/dropped by simply placing the optimized MRR at the corresponding side of the MBW.

3 Fabrication and Measurement

The designed ROADM chip was fabricated at Applied Nanotools on the SOI platform with a 220-nm-thick top silicon layer and a 2- μm -thick buried oxide layer. The SOI waveguides were fabricated with electron beam lithography followed by an inductively coupled plasma dry-etching process. A 1.5- μm -thick SiO_2 thin film was deposited above the silicon core layer as the upper cladding by utilizing the plasma-enhanced chemical vapor deposition process. Then the 200-nm thick titanium-tungsten (Ti/W) alloy microheater was deposited on top of the cladding. Figure 7(a) shows the microscope image of the whole fabricated photonic integrated circuit (PIC) with grating couplers at both input and output ends for efficient fiber-chip coupling, and the enlarged views of switches #0, #1, and #2 are shown in Figs. 7(b)–7(d). Here the microheaters were placed away from the coupling region of the MRRs, and thus the temperature variation has little impact to the evanescent coupling. In order to (de)multiplex the TE_0 , TE_1 , and TE_2 mode-channels, a pair of three-channel mode (de)multiplexers

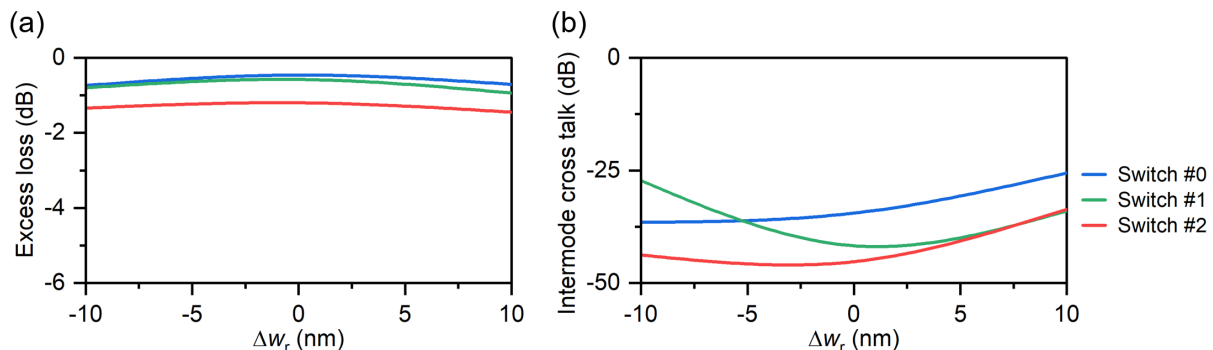


Fig. 6 Fabrication tolerance analysis. Analysis of the fabrication tolerance for switches #0, #1, and #2 when assuming that the core width w_r of the ring waveguide has a variation of ± 10 nm. (a) EL and (b) intermode cross talk.

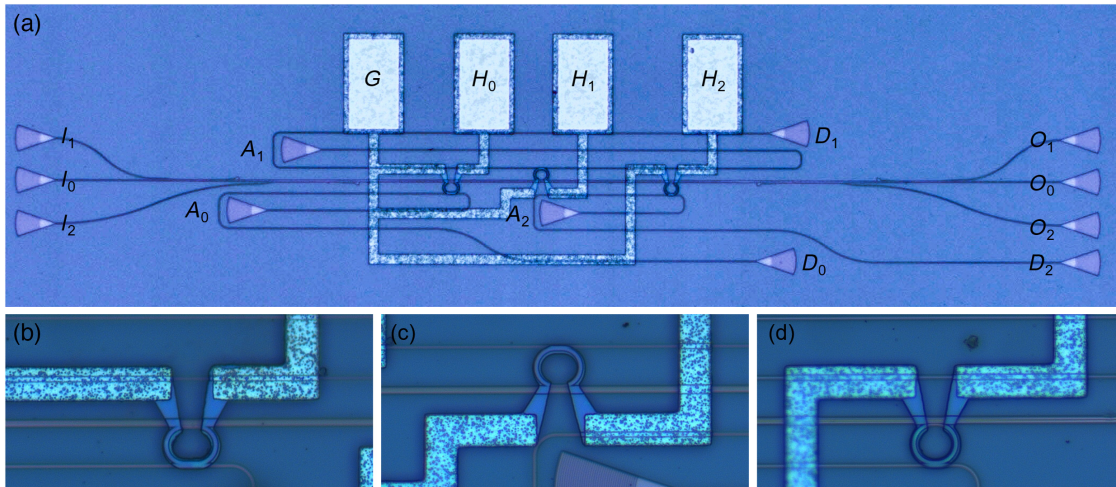


Fig. 7 Microscope image of the fabricated devices. (a) The whole fabricated PIC for switches #0, #1, and #2. The enlarged view of MRR switches (b) #0, (c) #1, and (d) #2.

based on dual-core adiabatic tapers³¹ were used. For the characterization of the fabricated PIC, a broadband amplified spontaneous emission (ASE) light was used as the light source and an optical spectrum analyzer (OSA) was used to record the transmission spectrum. The spectral response of the PIC was characterized by launching the light from input port I_i ($i = 0, 1$, and 2 , corresponding to the TE₀, TE₁, and TE₂ mode-channels) and monitoring the transmission at the drop port D_i ($i = 0, 1$, and 2). Here we mainly characterize the transmission from input port I_i to drop port D_i as well as the transmission from add port A_i to output port O_i .

Figures 8(a)–8(c) show the measured transmission spectra at drop port D_i in the wavelength range of 1530–1605 nm when light is launched from port I_i ($i = 0, 1$, and 2), respectively. The transmission is normalized with a straight single-mode waveguide fabricated on the same chip. Note that there are some wavelength deviations, which might be due to fabrication imperfections. Here the resonant wavelengths of the three MRRs are thermally tuned to be 1554.3 nm accordingly. The fabricated device shows a low EL from 0.6 to 2.7 dB over a broad wavelength range of 75 nm for all the channels. As shown in Figs. 8(a)–8(c), the FSR of the fabricated MRRs are ~ 14.76 ,

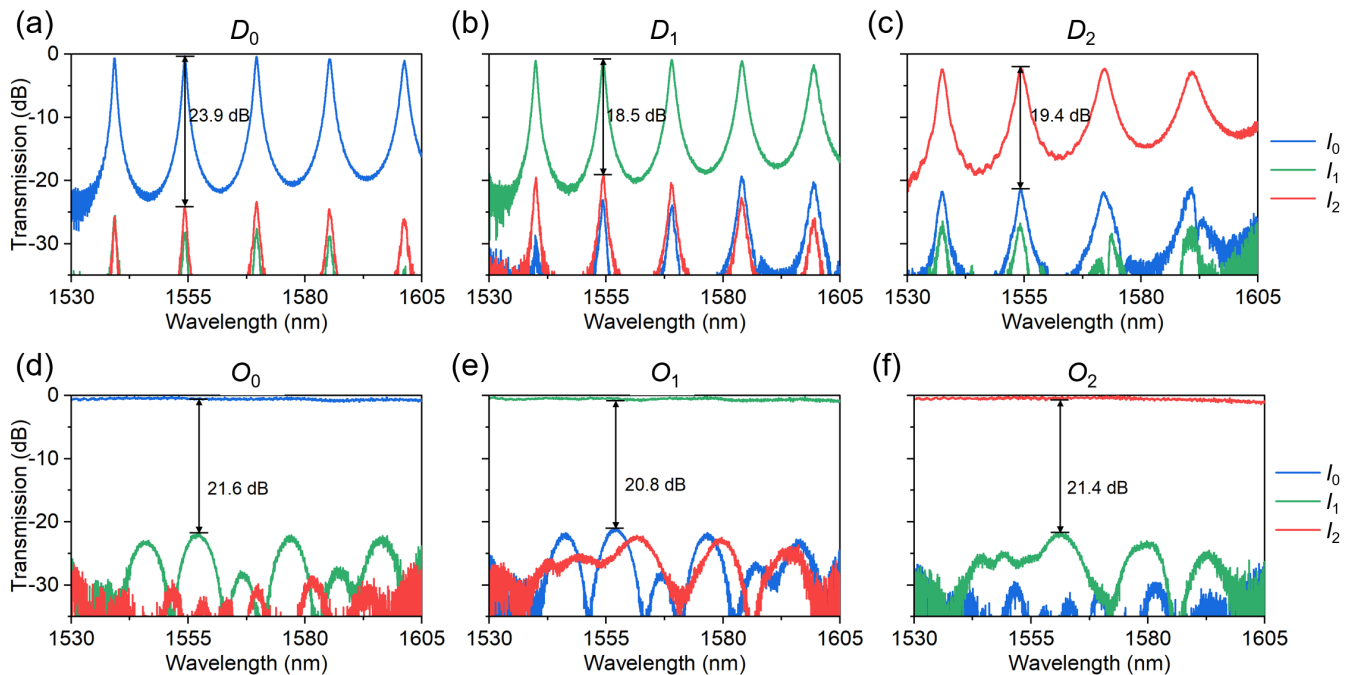


Fig. 8 Measured transmission results for the switches and the dual-core adiabatic taper mode (de)multiplexer. Normalized transmission spectra at drop port D_i covering a bandwidth of 1530–1605 nm when light is launched from port I_i [(a) $i = 0$, (b) $i = 1$, and (c) $i = 2$]. Normalized transmission spectra at output port O_i of the back-to-back dual-core adiabatic taper mode (de)multiplexer when light is launched from port I_i [(d) $i = 0$, (e) $i = 1$, and (f) $i = 2$].

14.65, and 16.14 nm; the slight difference is mainly caused by the fabrication deviation. The measured intermode cross talk is < -23.9 , -18.5 and -19.4 dB for switches #0, #1, and #2, respectively. As a comparison, we also characterize the performance of the back-to-back dual-core adiabatic taper mode (de) multiplexers when the TE_0 , TE_1 , and TE_2 modes are excited, as shown in Figs. 8(d)–8(f). It can be seen that the intermode cross talks of the mode (de)multiplexer are measured to be lower than -21.6 , -20.8 , and -21.4 dB in the wavelength range of 1530–1605 nm, which works well with the present design.

Figures 9(a)–9(c) show the transmission spectra of switches #0, #1, and #2 when the resonant wavelengths are thermally tuned with a channel spacing of $\Delta\lambda = 0.8$, 1.6, and 3.2 nm. It can be seen that when $\Delta\lambda$ is chosen as 3.2 nm, the cross talks of the adjacent wavelength-channels are -17.8 , -15.9 , and -10.1 dB, respectively. One might notice that the measured 3-dB bandwidth of switch #2 is larger than the simulation result, which might be caused by the increased coupling coefficients of MRRs due to fabrication variations. The desired 3-dB bandwidth can be achieved by updating the design and the fabrication when needed. The wavelength-channel cross talks can also be reduced by introducing the design of higher-order microrings, which enables box-like responses with lowered interchannel cross talk. Figure 10(a) shows the measured transmission at drop port D_1 of switch #1 when different electric powers are applied for the tuning of MRRs. The tuning efficiency of the MRRs is calculated and shown in Fig. 10(b). The wavelength

tuning efficiency is measured to be ≈ 0.141 nm/mW, and the whole FSR can be covered completely within the wavelength tuning range. Compared with the designs that can selectively access mode-/wavelength-carriers reported previously,^{26,27} the present ROADMs utilizing the modal field redistribution scheme possesses advantages of low insertion losses and low intermode cross talks, while no additional mode conversion devices are needed.

Furthermore, the experiment of data transmission in the fabricated PIC was carried out using the setup shown in Fig. 11(a). Two wavelength-channels (λ_1 and λ_2) were modulated by a high-speed electro-optic modulator, where the pulse pattern generators (PPGs) provided non-return-to-zero pseudo-random binary sequence signals to generate non-identical data with a bit rate of 30 Gbps for each wavelength-channel. The two modulated channels passed through a polarization controller (PC) and then multiplexed into a single mode fiber by a 3-dB coupler. The data carried by two wavelength-channels were then coupled into the fabricated chip from input port I_i ($i = 0, 1, \text{ and } 2$) through the grating coupler. In this way, the device was characterized with one of the mode-channels. As an example, here we choose to input the two-wavelength data (λ_1 and λ_2) from port I_0 corresponding to switch #0. Unfortunately, the characterization for the chip when operating with the three mode-channels simultaneously have not been carried out because the three-channel fiber array with channel spacing of $40 \mu\text{m}$ is not available in the lab. As a result, the eye diagram is given when operating

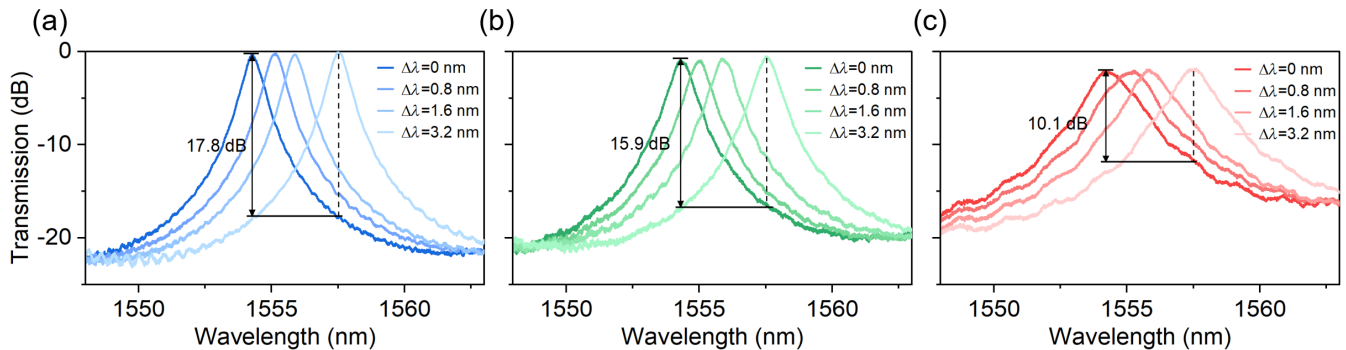


Fig. 9 Wavelength cross talk measurement of the switches. Transmission spectra of switches (a) #0, (b) #1, and (c) #2 when the resonant wavelengths are thermally tuned with a channel spacing of $\Delta\lambda = 0.8$, 1.6, and 3.2 nm.

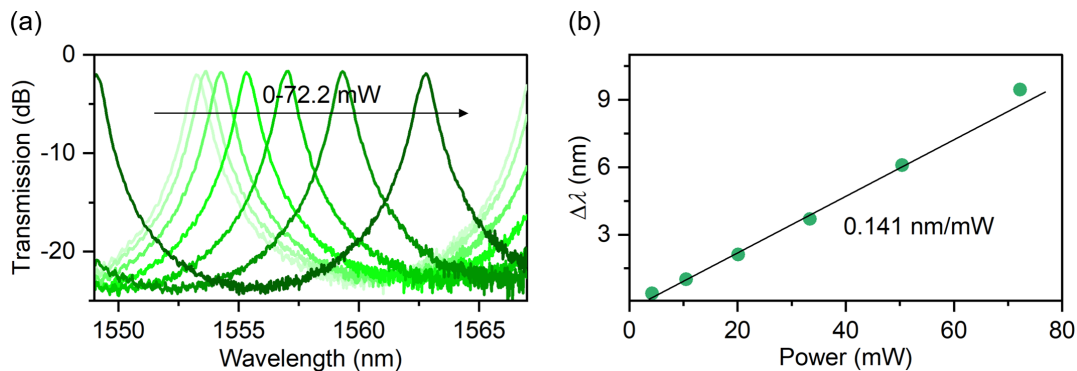


Fig. 10 Characterization of the thermal tuning performance. (a) Measured transmission of drop port D_1 when different electric powers are applied for the MRR tuning. (b) Calculated tuning efficiency of the MRRs.

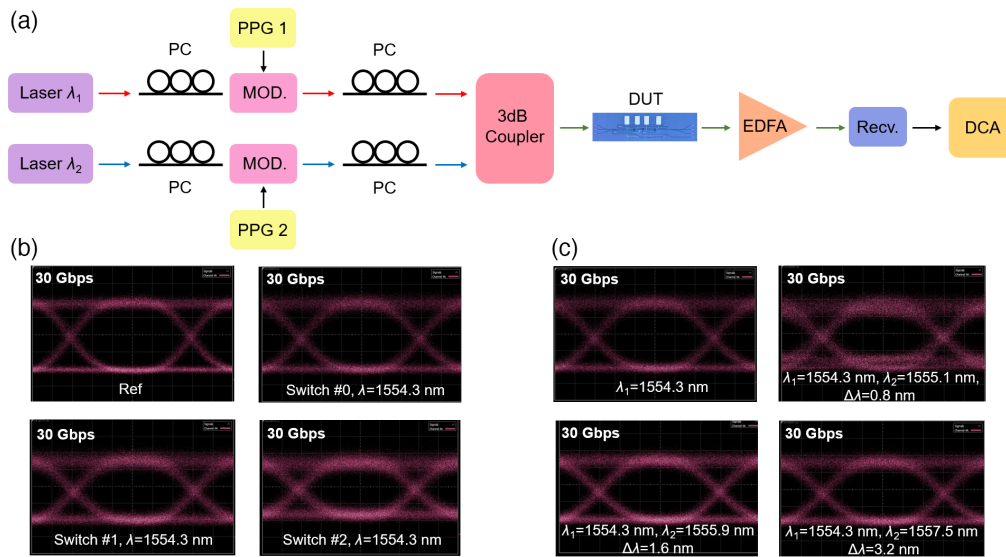


Fig. 11 Data transmission experiment. (a) Data transmission setup including tunable lasers, PCs, modulators (MOD), PPGs, device under test (DUT), erbium-doped fiber amplifier (EDFA), optical receiver (Recv), and digital communication analyzer (DCA). (b) Measured eye diagrams for data carried by each mode-channels, where a reference eye diagram of a straight single-mode waveguide is also shown. (c) Measured eye diagram when the input data are carried by two wavelength-channels with $\Delta\lambda = 0.8, 1.6,$ and 3.2 nm simultaneously.

with a single mode-channel. In a practical MDM transmission link, the intermode cross talk is the main contribution for the deterioration of the communication quality, which affects the quality of the eye diagram and the bit error rate.³² When multiple mode-channels are involved simultaneously, there is about a 0.1 to 2 dB power penalty introduced, corresponding to the intermode cross talk from -15 to -25 dB.^{20,33–35} Figure 11(b) shows the clear eye diagrams of switches #0, #1, and #2 for the TE_0 , TE_1 , and TE_2 mode-channels when operating at the wavelength of 1554.3 nm, respectively. Here the eye diagram of a straight single-mode waveguide is also shown as a reference. It can be seen that the measured eye diagrams of the three mode-channels are similar to that of the straight waveguide, indicating that the data pass through each mode-channel with high quality. The measured extinction ratios (ERs) are 9.0, 7.4, 6.4, and 5.5 dB, while the measured signal-to-noise ratios (SNRs) are 12.0, 8.8, 7.0, and 5.6 dB for the reference straight waveguide, switch #0, #1 and #2, respectively. Figure 11(c) shows the eye diagram of switch #0 as data carried by two wavelength-channels with a channel spacing of $\Delta\lambda = 0.8, 1.6,$ and 3.2 nm. Compared with the single wavelength-channel, the quality of the eye diagram is improved as the channel spacing is increased. The measured ERs are 5.9, 6.5, and 6.8 dB, while the measured SNRs are 4.9, 7.4, and 7.9 dB for the cases of $\Delta\lambda = 0.8, 1.6,$ and 3.2 nm, respectively. Consider the case with three mode-channels and four wavelength-channels: an aggregate data of 0.36 Tbit can be realized with a total of 12 channels. As demonstrated in Fig. 11, the present ROADM is promising for data switching and routing in hybrid MDM/WDM systems in the future.

4 Conclusion

In summary, we have proposed and demonstrated a silicon ROADM for hybrid MDM/WDM multiplexing by utilizing special modal field redistribution. In particular, SWG structures

have been utilized to engineer the refractive index, so that the launched TE_0 , TE_1 , and TE_2 modes are redistributed to be supermodes localized at different regions of the MBW. MRR wavelength-selective switches have been designed carefully and are placed at the corresponding side of the bus waveguide to selectively add/drop the target mode-channels. By tuning the resonant wavelength of each MRR, any wavelength-channels can also be switched and accessed selectively. With such devices, one can easily add/drop any mode-/wavelength-channel without affecting the other non-target channels. The simulated results show that the ELs are lower than 0.6, 0.7, and 1.3 dB, and the intermode cross talks are lower than -26.3 , -28.5 , and -39.3 dB for three mode-channels, respectively, around the central wavelength of 1550 nm. The fabricated device shows low ELs ranging from 0.6 to 2.7 dB for the TE_0 , TE_1 , and TE_2 modes at the resonant wavelength over a broad wavelength range of 75 nm. The intermode cross talks are < -23.9 , -18.5 , and -19.4 dB, respectively. The data transmission experiment of 30 Gbps/channel has also been demonstrated successfully. It is expected that the proposed ROADM provides an attractive route for data switching/routing in hybrid MDM/WDM systems.

Code, Data, and Materials Availability

The data that support the findings of this study are available from the corresponding author upon reasonable request.

Acknowledgments

This work was supported by the National Major Research and Development Program (Grant No. 2019YFB2203600); the National Science Fund for Distinguished Young Scholars (Grant No. 61725503); the National Natural Science Foundation of China (Grant Nos. 62125503, 91950205, 61961146003, and 62005238); the Zhejiang Provincial Natural Science

Foundation (Grant No. LD19F050001); The Fundamental Research Funds for the Central Universities; and The Leading Innovative and Entrepreneur Team Introduction Program of Zhejiang (Grant No. 2021R01001). The authors declare no conflicts of interest.

References

- R. Sabella, "Silicon photonics for 5G and future networks," *IEEE J. Sel. Top. Quantum Electron.* **26**(2), 1–11 (2020).
- G. Chen et al., "High-speed photodetectors on silicon photonics platform for optical interconnect," *Laser Photonics Rev.* **16**(12), 2200117 (2022).
- D. Dai and J. E. Bowers, "Silicon-based on-chip multiplexing technologies and devices for Peta-bit optical interconnects," *Nanophotonics* **3**(4–5), 283–311 (2014).
- Q. Cheng et al., "Recent advances in optical technologies for data centers: a review," *Optica* **5**(11), 1354–1370 (2018).
- T. Alexoudi et al., "Optics in computing: from photonic network-on-chip to chip-to-chip interconnects and disintegrated architectures," *J. Lightwave Technol.* **37**(2), 363–379 (2019).
- Y. Xiao, J. Zhang, and Y. Ji, "Integrated resource optimization with WDM-based fronthaul for multicast-service beam-forming in massive MIMO-enabled 5G networks," *Photonic Network Commun.* **37**(3), 349–360 (2019).
- J. A. Davis et al., "Silicon photonic chip for 16-channel wavelength division (de-)multiplexing in the O-band," *Opt. Express* **28**(16), 23620 (2020).
- P. G. Patki et al., "Recent progress on optical regeneration of wavelength-division-multiplexed data," *IEEE J. Sel. Top. Quantum Electron.* **27**(2), 1–12 (2021).
- H. Fukuda et al., "Silicon photonic circuit with polarization diversity," *Opt. Express* **16**(7), 4872 (2008).
- B. Shen et al., "An integrated-nanophotonics polarization beam-splitter with $2.4 \times 2.4 \mu\text{m}^2$ footprint," *Nat. Photonics* **9**(6), 378–382 (2015).
- S. Hinz et al., "Optical NRZ 2×10 Gbit/s polarisation division multiplex transmission with endless polarisation control driven by correlation signals," *Electron. Lett.* **36**(16), 1402 (2000).
- D. Guo et al., "Silicon polarization switch based on symmetric polarization splitter-rotators," *J. Semicond.* **40**(10), 100401 (2019).
- R. G. H. van Uden et al., "Ultra-high-density spatial division multiplexing with a few-mode multicore fibre," *Nat. Photonics* **8**(11), 865–870 (2014).
- H. Xu and Y. Shi, "Broadband nine-channel mode-division (de) multiplexer based on densely packed multimode waveguide arrays," *J. Lightwave Technol.* **35**(22), 4949–4953 (2017).
- Y. Liu et al., "Arbitrarily routed mode-division multiplexed photonic circuits for dense integration," *Nat. Commun.* **10**(1), 3263 (2019).
- Y. He et al., "Silicon high-order mode (de)multiplexer on single polarization," *J. Lightwave Technol.* **36**(24), 5746–5753 (2018).
- L. Xu et al., "Ultra-broadband and compact two-mode multiplexer based on subwavelength-grating-slot-assisted adiabatic coupler for the silicon-on-insulator platform," *J. Lightwave Technol.* **37**(23), 5790–5800 (2019).
- S. Wang et al., "On-chip reconfigurable optical add-drop multiplexer for hybrid wavelength/mode-division-multiplexing systems," *Opt. Lett.* **42**(14), 2802 (2017).
- Y. Tan et al., "Silicon-based hybrid demultiplexer for wavelength- and mode-division multiplexing," *Opt. Lett.* **43**(9), 1962 (2018).
- L.-W. Luo et al., "WDM-compatible mode-division multiplexing on a silicon chip," *Nat. Commun.* **5**(1), 3069 (2014).
- B. Stern et al., "On-chip mode-division multiplexing switch," *Optica* **2**(6), 530 (2015).
- H. Jia et al., "Mode-selective modulation by silicon microring resonators and mode multiplexers for on-chip optical interconnect," *Opt. Express* **27**(3), 2915 (2019).
- Y. Jiang et al., "A flexible and reconfigurable optical add-drop multiplexer for mode division multiplexing systems," *IEEE Photonics Technol. Lett.* **32**(24), 1515–1518 (2020).
- W. Zhao et al., "96-channel on-chip reconfigurable optical add-drop multiplexer for multidimensional multiplexing systems," *Nanophotonics* **11**(18), 4299–4313 (2022).
- Y. Dong et al., "Silicon-integrated high-speed mode and polarization switch-and-selector," *J. Semicond.* **43**(2), 022301 (2022).
- H. Xu et al., "Direct-access mode-division multiplexing switch for scalable on-chip multi-mode networks," *Nanophotonics* **10**(18), 4551–4566 (2021).
- J. Tan et al., "Arbitrary access to optical carriers in silicon photonic mode/wavelength hybrid division multiplexing circuits," *Opt. Lett.* **47**(14), 3531 (2022).
- K. H. R. Mojaver et al., "Mode sensitive SWG-based phase shifter for optical processors," in *IEEE Silicon Photonics Conf. (SiPhotonics)*, IEEE, pp. 1–2 (2023).
- X. Yi et al., "On-chip mode-selective manipulation based on the modal-field redistribution assisted with subwavelength grating structures," *Nanophotonics* **12**(9), 1809–1821 (2023).
- R. Halir et al., "Waveguide sub-wavelength structures: a review of principles and applications," *Laser Photonics Rev.* **9**(1), 25–49 (2015).
- D. Dai et al., "10-channel mode (de)multiplexer with dual polarizations," *Laser Photonics Rev.* **12**(1), 1700109 (2018).
- R. Ramaswami, K. Sivarajan, and G. Sasaki, *Optical Networks: A Practical Perspective*, Morgan Kaufmann (2009).
- Y. Ding et al., "On-chip two-mode division multiplexing using tapered directional coupler-based mode multiplexer and demultiplexer," *Opt. Express* **21**(8), 10376 (2013).
- R. B. Priti and O. Liboiron-Ladouceur, "A reconfigurable multi-mode demultiplexer/switch for mode-multiplexed silicon photonics interconnects," *IEEE J. Sel. Top. Quantum Electron.* **24**(6), 1–10 (2018).
- S. Zheng et al., "Silicon-based four-mode division multiplexing for chip-scale optical data transmission in the $2 \mu\text{m}$ waveband," *Photonics Res.* **7**(9), 1030 (2019).

Xiaolin Yi is currently pursuing her PhD at the College of Optical Science and Engineering, Zhejiang University, Hangzhou, China. Her current research interests include multimode silicon photonics and on-chip mode manipulation devices.

Weike Zhao is currently a postdoctoral fellow at the College of Optical Science and Engineering, Zhejiang University. He received his PhD from the University of Electronic Science and Technology of China. His current research interests include multimode silicon photonics and nonlinear optics.

Chenlei Li is currently a postdoctoral fellow at the College of Optical Science and Engineering, Zhejiang University. She received her PhD from Zhejiang University. Her current research interests include multimode silicon photonics and external cavity lasers.

Long Zhang is currently a postdoctoral fellow at the College of Optical Science and Engineering, Zhejiang University. He received his PhD from Zhejiang University. His current research interests include multimode silicon photonics and on-chip spectrometers.

Yuluan Xiang received his PhD from Zhejiang University. He currently works as an engineer at Robsense Co., Ltd. His research interests include silicon-integrated avalanche photodetectors.

Chaoyue Liu received his PhD from Zhejiang University. He currently works as an engineer at Changguang Chenxin Microelectronics Co., Ltd. His research interests include silicon-integrated photodetectors and optical architecture design.

Yaocheng Shi is currently a professor at Zhejiang University and mainly works on silicon photonics. He has published several refereed international journal papers.

Liu Liu is currently a professor at Zhejiang University and mainly works on high-performance LNOI modulators. He has published several refereed international journal papers.

Daoxin Dai is currently the QIUSHI Distinguished Professor at Zhejiang University and mainly works on silicon photonics. He has published several refereed international journal papers. He is one of the most cited Chinese researchers from 2015 to 2021 (Elsevier).